Research Article | Vol. 30, No. 17 / 15 Aug 2022 / Optics Express 30696
Optics EXPRESS

Enhanced graphene surface plasmonics through incorporation into metallic nanostructures

YONGLIANG DONG[1] AND PRABHAKAR R. BANDARU[1,2,*]

[1]Program in Material Science, Department of Mechanical Engineering, University of California, San Diego, La Jolla, CA 92092, USA
[2]Department of Electrical Engineering, University of California, San Diego, La Jolla, CA 92092, USA
*pbandaru@ucsd.edu

Abstract: A methodology for enhancing the surface plasmon polariton (SPP) resonance associated with graphene, through nanoscale metal-dielectric-metal (MDM) gaps, is proposed. The modulation of the resonances, in the range of 0.7 μm to 1 μm was done through tuning the carrier density in graphene and has been shown to be of potential utility for surface analyte sensing. It was shown, from finite element simulations in the frequency domain, that the related *hybrid* SPP modes could be clearly delineated in far field spectroscopy.

1. Introduction

The phenomena related to surface plasmon polariton (SPP) resonances, based on the collective oscillation of carriers excited by incident electromagnetic (EM) waves, has been well explored at metal (negative refractive index: n_m)-dielectric (positive refractive index: n_d) interfaces [1,2]. The high sensitivity of the resonance to the refractive index difference (Δn), has resulted in the use of SPP-based phenomena for scientific insights into near-field EM interactions as well as technological applications, such as label-free diagnostics and sensing [3–6]. For instance, the manifestation of distinct SPP mode varieties [7–9], *e.g.,* in metallic nanogaps incorporating Fabry-Perot (F-P) resonances and the related peak splitting in the far field [10], enabling a larger spectral range has been previously considered. The magnitude of such interactions is determined by the geometry and material constituting the metal/dielectric/metal (MDM) gaps, of size less than the incident wavelength (λ_0) [11]. Such gaps could be fabricated by lithography or through using the spaces between metallic nanocubes [11–13].

One aim of the present work was to bring forth the characteristic utility of low dimensional materials, such as graphene, integrated with such MDM gratings for the further modulation of F-P based SPP resonances [14–20]. The ability to vary the carrier density of graphene by orders of magnitude, through electronic gating [16] or chemical doping could be harnessed in this regard. For instance, with increased carrier density, the in-plane dielectric constant ($\varepsilon_{||}$) of graphene may be made negative in the near-IR regime (with λ_0 in the range of 0.7 μm to 1 μm) and helps support a graphene SPP (GrSPP) at the graphene/dielectric interface [16]. The formation of such a GrSPP has been previously verified through near field spectroscopy [16].

Here, we indicate the coupling of the GrSPP with F-P like MDM gap resonances, and their spectroscopic signature. To manifest and tune the GrSPP [17,20], a carrier density in the range of 0.75×10^{14} cm^{-2} to 2×10^{14} cm^{-2} was chosen - implying a Fermi energy (μ) in the range of 1 eV to 1.7 eV. While it has previously been shown that the μ of the graphene could be tuned through using metal nanoparticles [21], the use of metallic material implies loss and it would be better to use graphene alone. Previous work on the modulation of the GrSPP through metallic gratings, considered the coupling of the localized resonances *via* the magnetic polaritons with the GrSPP, at larger wavelengths ($\lambda_0 \sim 10$ μm) [22] as a function of grating geometry [23]. The

#461754 https://doi.org/10.1364/OE.461754
Journal © 2022 Received 21 Apr 2022; revised 6 Jun 2022; accepted 7 Jun 2022; published 8 Aug 2022

Optics EXPRESS

influence of conformational changes of the graphene overlaid on metallic gratings on the GrSPP was revealed through a *red* shift in the absorption peak at $\lambda_0 \sim 3$ μm, with μ of the order of 0.3 eV [24], indicating a frequency dependency to the GrSPP phase shift [25]. Here, we propose the use of hexagonal boron nitride (hBN) to reduce wrinkles while promoting an ultra-flat, loosely bound configuration for the graphene [26]. Considering smaller λ_0 values and higher μ values, our models cover a much larger range of μ of up to 1.7 eV and have observed blue shifts of the MDM SPP due to the presence of graphene. Moreover, the graphene is placed underneath the metal-dielectric-metal grating, for greater ease of fabrication. We also suggest a new application considering the GrSPP - MDM SPP interactions and related tunability, for sensor modality.

We have conducted finite-element frequency simulation by COMSOL, for comparing both metal SPP and graphene SPP in the Ag/air/Ag grating – corresponding to the MDM configuration with graphene at the bottom, as shown in Fig. 1(a). In practice, a graphene layer may be isolated, through etching it off the copper substrate, and subsequent placement of the layer through a wet transfer assisted transfer onto hBN placed on top of a Si/SiO_2 substrate. An MDM grating, with a defined periodicity (p), grating height (h), width (w), and gap width (g): Fig. 1(b), could be fabricated on the graphene through electron-beam lithography-based procedures. It is also plausible, as indicated previously, that the gaps related to the MDM grating could be realized through using the spaces between metallic nanocubes, synthesized through chemical processing [11–13].

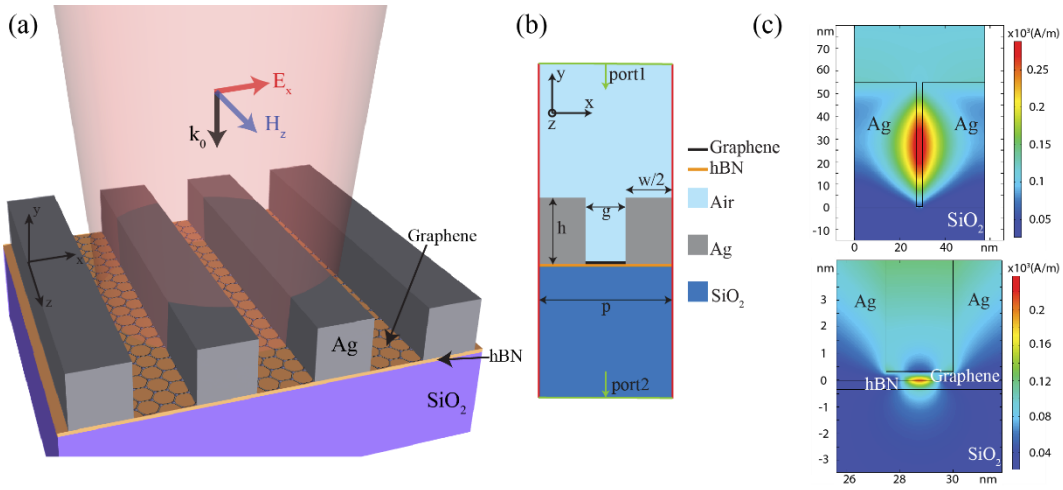

Fig. 1. (a) A schematic of the metallic (Ag) grating on top of graphene with hBN underlayer and SiO_2/Si substrate; (b) The unit cell used for the simulation. The geometric parameters, for the simulation, are the periodicity (p), grating height (h), width (w), and gap width (g); (c) The magnetic field magnitude ($|H_z|$) for MDM SPP resonance in the Ag/air/Ag (M/D/M) slit *top*, and GrSPP resonance: *bottom*.

The periodic unit cell for the simulation is indicated through a domain annotated in Fig. 1 (b). The *top*(/*bottom*) indicates the input (/output) ports: 1 (/2), for the simulation. A p-polarized plane wave (with an electric field orientation in the x-y plane: $E_{x,\,y}$) is incident vertically and excites F-P based MDM SPP modes and GrSPP modes within the thin vertical slit. Such an aspect is manifested, for instance, through the output magnetic field magnitude ($|H_z|$) as related to the resonances of F-P like MDM SPP (Fig. 1 (c): top) and GrSPP (Fig. 1 (c): bottom). A clear coupling and energy splitting between MDM F-P SPP and related Gr SPP was observed. The resultant modulation of the coupled resonance modes may be correlated to a change in the effective refractive index (Δn) of the graphene integrated MDM structure.

Optics EXPRESS

2. Resonances related to the metal-dielectric-metal (MDM) gaps

The occurrence of the SPP was investigated in terms of the geometrical parameters, related to the MDM geometry, as indicated in Fig. 1(b). For the metallic grating with subwavelength periodicity ($p \ll \lambda_0$), the SPP in the MDM gap is termed F-P *like* from fulfilling the resonance condition: $\beta_{MDM} \cdot h \sim m\pi$, where β_{MDM} is the wavevector of the MDM SPP and m is an integer representing the order of the resonance: Fig. 2 (a). Such a condition can be estimated by the MDM gap mode relations [10], with enhancement of the SPP resonance brought about by constructive interference inside the slit as indicated through the $|H_z|$ maximum at the slit center: Fig. 1 (c): *top*). We had previously investigated the geometry dependence of the β_{MDM} and the related resonances [10]. Here, we indicate the resonance peaks obtained in the absorption spectrum of the grating structure.

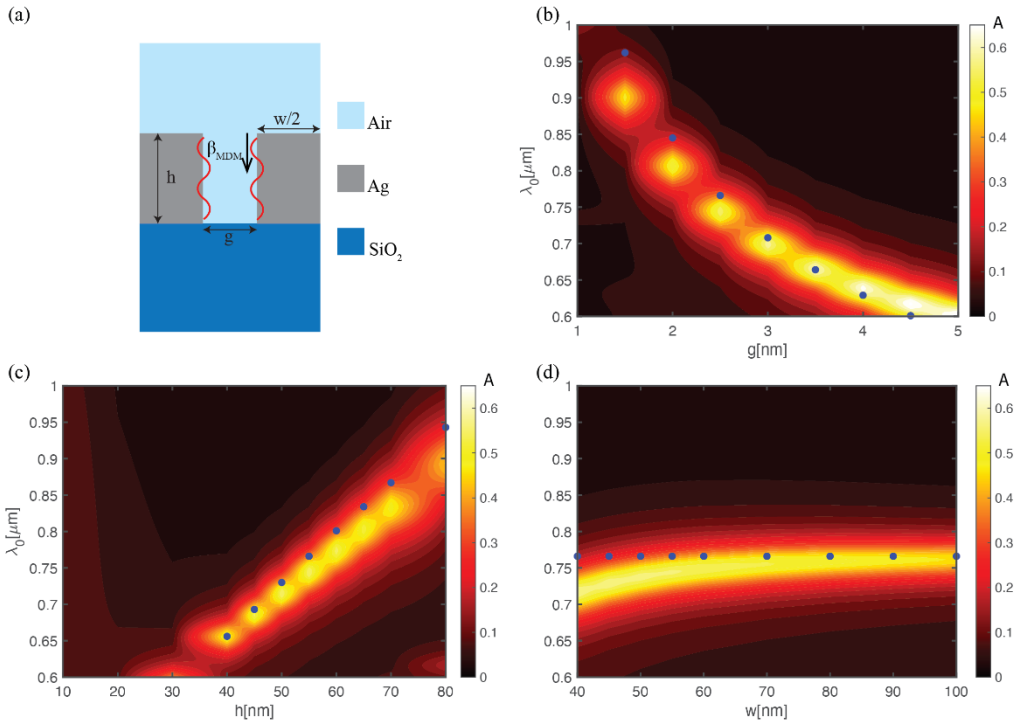

Fig. 2. (a) The unit cell, used for simulating the MDM SPP resonance, with the related SPP propagating along the vertical direction; The variation of the absorption (A) as a function of the grating structure geometry, with (b) g, with $h = w = 55$ nm; (c) h, with $w = 55$ nm and $g = 2.5$ nm; and (d) w with $h = 55$ nm, $g = 2.5$ nm. The blue dots are in correspondence MDM SPP resonance condition $\beta_{MDM} \cdot h \sim m\pi$, associated with the β_{MDM} dispersion indicated in Fig. S1(a) of Supplement 1.

In Fig. 2 (b) the spectral variation of the far field absorption (A) with the grating width: g, is shown. The h and w were set at ~ 55 nm – a value corresponding to commercial Ag nanocube length scales (*e.g.,* from nanoComposix.com), which could support MDM F-P like resonances [12]. The resonance peak (blue dots) variation with g, considered in accord with the β_{MDM} dispersion indicated in Fig. S1(a) of Supplement 1, is also shown. It was seen that the peak shifts through reducing g (say, from 5 nm to 1 nm) substantially from ~ 0.6 μm to ~ 1 μm. A smaller g implies a shift to higher λ_0 and is associated with decreasing A due to the smaller MDM gap volume [10]. A higher h implies a shift to a smaller β_{MDM}/larger λ_0 : see Fig. 2 (c)

Optics EXPRESS

from $\beta_{MDM} \cdot h \sim m\pi$. The influence of the grating width (w) on the resonance shift, as indicated in Fig. 2 (d), is less pronounced. The interference between adjacent MDM slits at reduced w may be expected to yield a blue shift.

3. Excitation of GrSPP resonances in confined single-layer graphene

Integrating graphene into the metallic grating adds a new *tunable* degree of freedom for further modulating SPP resonances. As is well known, the tuning of the graphene carrier density to vary the electrical conductivity coupled with the all-surface characteristic of the graphene enables specificity and sensitivity [14–21,27–29], that may be utilized for sensing applications. In our simulations, an atomically thin single layer graphene (SLG) of thickness $t = 0.34$ nm [30], *e.g.,* in the form of graphene nanoribbons (GNR) was placed at the bottom of the Ag grating constituted MDM gap, with an underlying layer of hBN: Fig. 3(a) The hBN has been typically used for atomically smooth and ultra-flat graphene surfaces [26]. The MDM related barriers help for the confinement of GrSPP in the gap following its excitation by the *p*-polarized illumination.

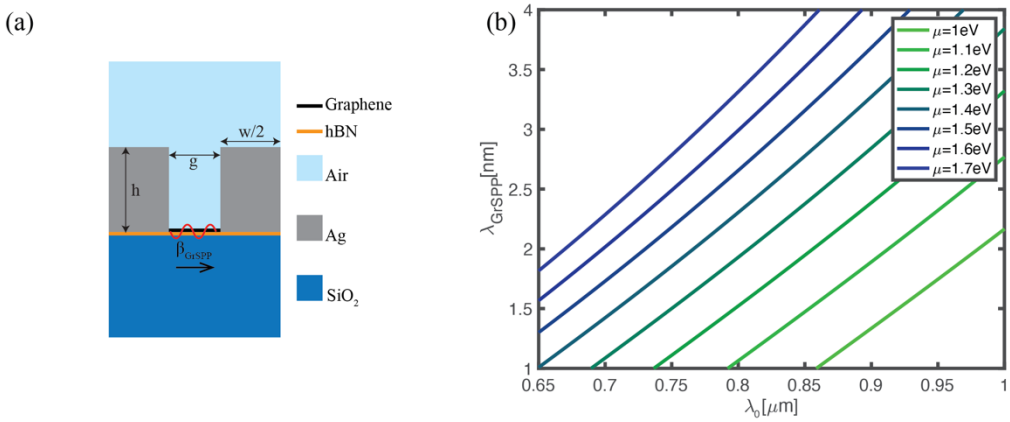

Fig. 3. (a) The simulation unit cell incorporating the single layer graphene (SLG) overlaid on hBN on a SiO_2/Si substrate. The GrSPP propagates along the SLG surface; (b) Estimation of graphene SPP wavelength (λ_{GrSPP}) with respect to the λ_0 for μ in the range of 1 eV to 1.7 eV.

In this study, the carrier density of graphene was modulated over a range of 0.75×10^{14}cm^{-2} to 2×10^{14}cm^{-2}, with μ varying in the range of 1 eV to 1.7 eV (Supplement 1 Fig. S2(a)), for tuning the GrSPP response in the near-IR. The carrier density of graphene may be tuned through an (i) applied voltage, or through (ii) chemical doping, as indicated in the introductory sections. For instance, a negative (/positive) gate voltage applied to the back of the Si substrate would decrease (/increase) the carrier density [31]. Alternately, the use of electron donor (/acceptor) molecules, e.g., aniline and tetrathiafulvalene: TTF) (/oxygen or tetracyanoethylene: TCNE) could increase (/decrease) the carrier density of the graphene. Such an aspect for manifesting the surface plasmons through modulations of the carrier density has been extensively indicated in literature [16]. Consequently, the graphene in-plane optical conductivity: $\sigma = \sigma_{intra} + \sigma_{inter}$; involves both *intra*-band and *inter*-band contributions from electron-phonon scattering and electronic energy level transitions, respectively and is indicated as a function of μ, through the following relations [27–29]:

$$\begin{aligned} \sigma_{intra} &= \frac{2ie^2k_BT}{\hbar^2\pi(\omega+i\Gamma)} \ln\left[2\cosh\left(\frac{\mu}{2k_BT}\right)\right] \\ \sigma_{inter} &= \frac{e^2}{4\hbar}\left[\frac{1}{2} + \frac{1}{\pi}\tan^{-1}\left(\frac{\hbar\omega-2\mu}{2k_BT}\right) - \frac{i}{2\pi}\ln\frac{(\hbar\omega-2\mu)^2}{(\hbar\omega-2\mu)^2+(2k_BT)^2}\right] \end{aligned} \quad (1)$$

Optics EXPRESS

Here, e is the unit of elementary electronic charge, ω is the frequency of incident light ($\omega=2\pi c/\lambda_0$), Γ is the charge carrier scattering rate of ~ 10 ps^{-1} [32] and T the temperature (300K) [29]. The in-plane dielectric constant $\varepsilon_{||}$ ($= 1 + i\sigma/\varepsilon_0\omega t$) for SLG was obtained from a thin slab model [29]. The out-of-plane dielectric constant ($\varepsilon_{\perp}$) was assumed to be 6.9 as a constant since the charge oscillation is limited to the atomic plane [33]. The calculated real and imaginary parts of the $\varepsilon_{||}$ are plotted in Supplement 1 Figs. S2(b),(c), over a range of μ from 1 eV to 1.7 eV. The negative Re $\{\varepsilon_{||}\}$ was observed with λ_0 from 0.7 μm to 1 μm, and is crucial for the GrSPP mode at the graphene-dielectric (where $\varepsilon > 0$) interface. To further understand the GrSPP characteristics, a λ_0-λ_{GrSPP} relationship was computed. Considering the SLG enclosed by two dielectrics (ε_1, ε_2), such as air($\varepsilon_1 = 1$) and anisotropic hBN($\varepsilon_{2,||}$=4.97 with $\varepsilon_{2,\perp}$=2.89 [34], and incident TM polarization, we have $\beta_{GrSPP} = 2\pi/\lambda_{GrSPP} = i\varepsilon_0(\varepsilon_1+\varepsilon_2)\omega/\sigma$ [29]. The resultant plot in Fig. 3(b) shows that the GrSPP has wavelength λ_{GrSPP} two orders of magnitude smaller than the λ_0, implying significant confinement of the related SPP. Such an aspect is in accord with the notion that while the GrSPP can be excited, there is nominally negligible response in the far field spectrum due to the near field confinement. Such a response is indicated at the bottom of Fig. 4 (a) through the relatively flat green feature. However, the integration of the graphene with an MDM will be now shown to yield significant spectral modulation.

4. Probing single-layer graphene SPP coupled to MDM resonances

We investigate the influence of the GrSPP resonance signal in the far-field spectrum through its modulation of the F-P resonance related to the MDM structure, considering the configuration of Fig. 3(a). Here, the metallic grating serves to support the F-P like mode and presents a reflective boundary for the GrSPP. The confined GrSPP forms standing wave resonances, at the bottom of the gap. When the GrSPP and MDM F-P like SPP resonances are comparable in energy, the mutual coupling of the related excitations would need to be considered [10]. This may occur through the simultaneous excitation of *both* the GrSPP and MDM F-P like SPP arising from the redistribution of electrical charges proximate to the graphene and Ag interface [10].

In Fig. 4(a), a comparison of the absorption in the MDM grating (*red curve*) with that for the grating with the SLG at the bottom of the gap (*blue curve*) is shown, for $\mu = 1.5$ eV and $g = 2.5$ nm. While only one SPP resonance peak, corresponding to the MDM F-P like SPP mode, is apparent in the former case, with graphene there are two peaks. The coupling between GrSPP and F-P like MDM mode is evident. For the GrSPP, the resonance follows the criteria:

$$\beta_{GrSPP} \cdot g \approx 2p\pi \tag{2}$$

Here, p is an integer and the condition in Eqn. (2) implies coupling to the incident light, related to the electric field component: E_y as further elucidated, through Fig. S3, in Supplement 1. The GrSPP resonance (along x) is antisymmetric, implying that the electric field on both surfaces of graphene is out of phase - see Figs. S3(b),(c) in Supplement 1. As a result, the constructive interference only occurs for modes with even values of p [35]. From the dispersion relationship of GrSPP at a given μ: Fig. 3(b) and the MDM SPP: Fig. S1(a), we estimate the $\beta_{GrSPP} = 2856$ μm^{-1} $\sim (2\pi/2.5\text{nm})$ and $\beta_{MDM} \sim 50\mu\text{m}^{-1} \sim (\pi/55\text{nm})$ at $\lambda_0 \sim 0.75\mu$m, fulfilling the condition for the occurrence of both the MDM and graphene related SPP resonances: $\beta_{MDM} \cdot h \sim \pi$ and $\beta_{GrSPP} \cdot g \sim 2\pi$ (with $h = 55$ nm and $g = 2.5$ nm).

The double peak feature may be understood through a resonant energy splitting criteria [10]. With both MDM F-P like SPP and GrSPP (μ =1.5 eV) resonances coinciding at $\lambda_0 \sim 0.75$ μm, a resonance peak splitting was observed with two absorption peaks at 0.722 μm and 0.756 μm, in Fig. 4(a). By tuning the μ in the range of 1 eV to 1.7 eV, a modulation of the GrSPP and MDM SPP resonances is indicated: Fig. 4(b). The peaks on the right (downward triangles), when the μ < 1.5 eV represents the GrSPP resonance following $\beta_{GrSPP} \cdot g \sim 2\pi$. For instance, with $\mu = 1.1$ eV, at $\lambda_0 \sim 0.9$ μm we have $\lambda_{GrSPP} \sim 2.3$ nm, and the observation of a small GrSPP resonance peak in

Optics EXPRESS

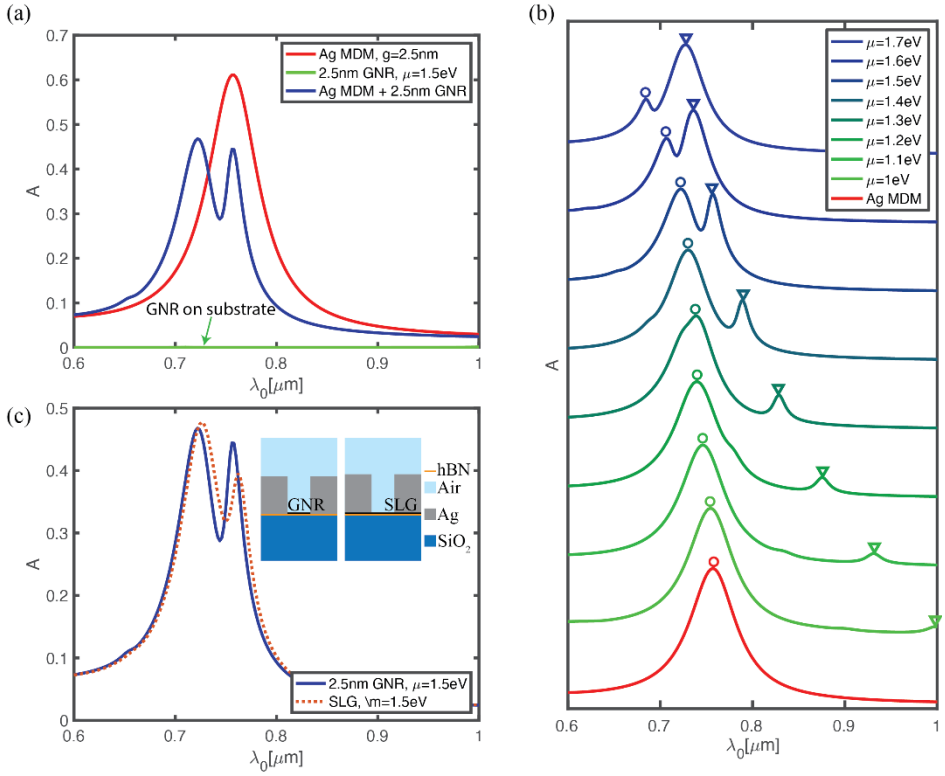

Fig. 4. (a)The absorption (A) vs λ_0 of the metallic grating *with* and *without* a 2.5 nm GNR ($\mu = 1.5$ eV) at the bottom of the MDM gap ($h = w = 55$ nm, $g = 2.5$ nm); The absorption related to the GNR on a substrate - without metallic grating is also indicated through the *flat green* feature at the bottom. (b) The absorption spectra for GNR in the MDM structure, with μ varying from 1 eV to 1.7 eV; (c) Spectral variation of the absorption, for GNR in the gap (*blue*) and the SLG under the metallic grating (*red dotted*) – see right image in the *inset*, showing similar resonance behavior.

the absorption spectrum. However, with an increased $\mu = 1.5$ eV, the related GrSPP peak occurs at $\lambda_0 \sim 0.76$ μm with a seven-fold increase in the absorption, due to coupling with the MDM F-P like SPP. The blue shift of the MDM SPP with increasing μ indicates the enhanced influence of the graphene and is further discussed in Section S4 of Supplement 1.

Generally, the placement of GNR with precise control of metallic structures on top is practically difficult. Alternatively, a complete single layer of graphene (SLG) can be used as shown in the *right inset* figure of Fig. 4(c). The related SLG SPP mode interaction with the F-P like MDM gap mode is indicated through the *red dotted* trace in Fig. 4(c). However, the absorption peak splitting corresponding to the GrSPP, and MDM SPP interaction seems less pronounced compared to the GNR case: Fig. 4(c). The latter is related to a more tightly confined GrSPP resonance as defined through *both* the graphene as well as the metal edges.

5. Deployment of the *hybrid* GrSPP – MDM SPP interaction for transducing refractive index changes and application for analyte sensing

Taking advantage of the tunability of the GrSPP - MDM SPP interaction, we propose its utilization for a sensor modality. We define the sensitivity of the *hybrid* SPP resonance through the peak shift (in wavelength units) with respect to a given refractive index (n) change, in units of nm/RIU,

Optics EXPRESS

where RIU: refractive index unit. As an example, consider the SLG (say, of $\mu = 1.5$ eV) embedded under the Ag grating structure with $g = 10$ nm, $w = 80$ nm, $h = 80$ nm, the chosen parameters chosen for length scales achievable through lithography. With the analyte (say, of thickness ~ 1 nm) adsorbed on the graphene surface: Fig. 5(a) inset, the effective n of the assembly would be manifested in the observed spectrum. A varying analyte characteristic *e.g.,* the n_{analyte}, from ~ 1.3 (say, glucose) to 1.7 (say, for mutagens such as diiodomethane) would be indicated through a shift of the SPP resonances. The spectral variation of the absorption is plotted as a function of the n_{analyte} in Fig. 5(a). Three absorption peaks were observed at ~ 0.7 μm, ~ 0.8 μm and ~ 0.9 μm, and labeled as MDM, GrSPP1 and GrSPP2, respectively. The change of the resonance peak position with respect to the n_{analyte}, is indicated in Fig. 5(b). The GrSPP related peaks show a ten-fold higher sensitivity (GrSPP1~ 130 nm/RIU at λ_0~ 0.8μm and GrSPP2 ~ 157.6 nm/RIU at λ_0~ 0.9μm) compared to the MDM SPP resonance (~ 17.2 nm/RIU at λ_0~ 0.7μm). The utility of the GrSPP in concert with the SPPs arising from MDM based resonances for sensing applications is hence indicated. A further investigation of GrSPP based sensing, with respect to MDM geometry, is discussed in Section 5 of Supplement 1.

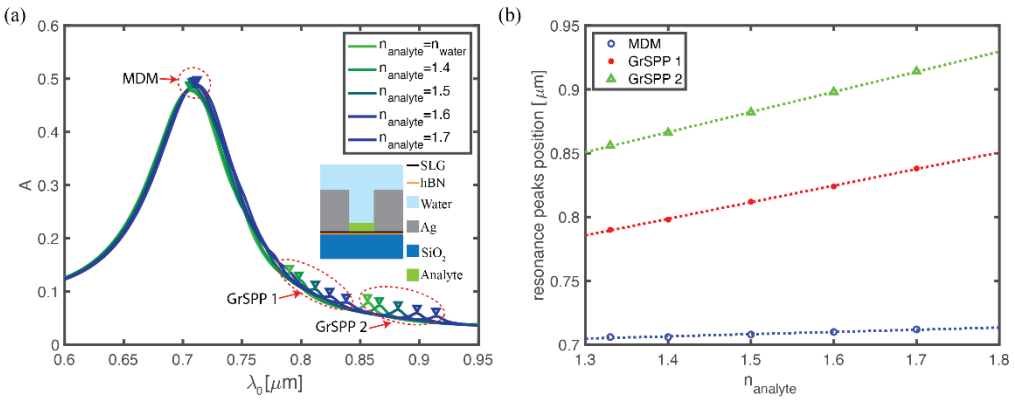

Fig. 5. (a) The spectral variation of the absorption (A) as a function of an analyte ($n_{\text{analyte,}}$) –as considered through the refractive index. Three resonance peaks (MDM, GrSPP1 and GrSPP2) were observed; (b) The respective resonance peak shift as a function of the change in the refractive index unit (RIU) of the analyte *i.e.,* the MDM: 17.2 nm/RIU, GrSPP1:130 nm/RIU and GrSPP2: 157.6 nm/RIU, may be used for transducing the index changes of the analyte.

6. Conclusion

We have indicated that the hybrid coupling of SPP modes, arising from the GrSPP and the MDM SPP, can be modulated by tuning the μ of the graphene, through carrier density variation. A seven-fold enhancement of the GrSPP resonance peak was observed in the far field spectra in the near - IR regime, when a supporting MDM based grating was deployed. The hybrid GrSPP-MDM SPP platform can be used for enhanced signal as well as larger sensitivity, *e.g.,* an order of magnitude larger spectral change was obtained for a given refractive index unit change. The related principles offer possibility for analyte sensing at the nanometer scale.

Funding. National Science Foundation (NSF: CBET 1606192).

Disclosures. The authors declare no conflicts of interest.

Data availability. Data underlying the results presented in this paper are not publicly available at this time but may be obtained from the authors upon reasonable request.

Supplemental document. See Supplement 1 for supporting content.

Optics EXPRESS

References

1. S.A. Maier, *Plasmonics: fundamentals and applications* (Springer Science & Business Media, 2007).
2. W. L. Barnes, A. Dereux, and T. W. Ebbesen, "Surface plasmon subwavelength optics," Nature **424**(6950), 824–830 (2003).
3. K. A. Willets and R. P. Van Duyne, "Localized surface plasmon resonance spectroscopy and sensing," Annu. Rev. Phys. Chem. **58**(1), 267–297 (2007).
4. H. H. Nguyen, J. Park, S. Kang, and M. Kim, "Surface plasmon resonance: a versatile technique for biosensor applications," Sensors **15**(5), 10481–10510 (2015).
5. Y. Zhao, R.-j. Tong, F. Xia, and Y. Peng, "Current status of optical fiber biosensor based on surface plasmon resonance," Biosens. Bioelectron. **142**, 111505 (2019).
6. J. Dostalek, J. Čtyroky, J. Homola, E. Brynda, M. Skalský, P. Nekvindova, J. Špirková, J. Škvor, and J. Schröfel, "Surface plasmon resonance biosensor based on integrated optical waveguide," Sens. Actuators, B **76**(1-3), 8–12 (2001).
7. Z. Yong, S. Zhang, C. Gong, and S. He, "Narrow band perfect absorber for maximum localized magnetic and electric field enhancement and sensing applications," Sci. Rep. **6**(1), 24063 (2016).
8. L. Lin and Y. Zheng, "Optimizing plasmonic nanoantennas via coordinated multiple coupling," Sci. Rep. **5**(1), 14788 (2015).
9. W. Zhou, J. Y. Suh, Y. Hua, and T. W. Odom, "Hybridization of localized and guided modes in 2d metal–insulator–metal nanocavity arrays," J. Phys. Chem. C **117**(6), 2541–2546 (2013).
10. Y. Dong and P. R. Bandaru, "Interaction and hybridization of orthogonal fabry-pérot like surface plasmon modes in metal-dielectric grating structures," Opt. Express **28**(3), 3541–3551 (2020).
11. J. Le Perchec, P. Quemerais, A. Barbara, and T. Lopez-Rios, "Why metallic surfaces with grooves a few nanometers deep and wide may strongly absorb visible light," Phys. Rev. Lett. **100**(6), 066408 (2008).
12. A. Moreau, C. Ciracì, J. J. Mock, R. T. Hill, Q. Wang, B. J. Wiley, A. Chilkoti, and D. R. Smith, "Controlled-reflectance surfaces with film-coupled colloidal nanoantennas," Nature **492**(7427), 86–89 (2012).
13. J. B. Lassiter, F. McGuire, J. J. Mock, C. Ciracì, R. T. Hill, B. J. Wiley, A. Chilkoti, and D. R. Smith, "Plasmonic waveguide modes of film-coupled metallic nanocubes," Nano Lett. **13**(12), 5866–5872 (2013).
14. L. Wu, H. Chu, W. Koh, and E. Li, "Highly sensitive graphene biosensors based on surface plasmon resonance," Opt. Express **18**(14), 14395–14400 (2010).
15. K. N. Shushama, M. M. Rana, R. Inum, and M. B. Hossain, "Sensitivity enhancement of graphene coated surface plasmon resonance biosensor," Opt. Quantum Electron. **49**(11), 381 (2017).
16. Q. Zhang, X. Li, M.M. Hossain, Y. Xue, J. Zhang, J. Song, J. Liu, M.D. Turner, S. Fan, Q. Bao, and M. Gu, "Graphene surface plasmons at the near-infrared optical regime," Sci. Rep. **4**(1), 6559 (2015).
17. S. Zeng, K. V. Sreekanth, J. Shang, T. Yu, C. K. Chen, F. Yin, D. Baillargeat, P. Coquet, H. P. Ho, A. V. Kabashin, and K. T. Yong, "Graphene–gold metasurface architectures for ultrasensitive plasmonic biosensing," Adv. Mater. **27**(40), 6163–6169 (2015).
18. H. Zhang, D. Song, S. Gao, J. Zhang, H. Zhang, and Y. Sun, "Novel spr biosensors based on metal nanoparticles decorated with graphene for immunoassay," Sens. Actuators, B **188**, 548–554 (2013).
19. P. K. Maharana, R. Jha, and P. Padhy, "On the electric field enhancement and performance of spr gas sensor based on graphene for visible and near infrared," Sens. Actuators, B **207**, 117–122 (2015).
20. A. Verma, A. Prakash, and R. Tripathi, "Sensitivity enhancement of surface plasmon resonance biosensor using graphene and air gap," Opt. Commun. **357**, 106–112 (2015).
21. Y. Wan, L. Deng, L. Wang, M. Yang, and Y. Wang, "Modulation of visible and near-infrared surface plasmon resonance of au nanoparticles based on highly doped graphene," Plasmonics **12**(5), 1317–1324 (2017).
22. B. Zhao and Z. M. Zhang, "Strong plasmonic coupling between graphene ribbon array and metal gratings," ACS Photonics **2**(11), 1611–1618 (2015).
23. B. Zhao, J. M. Zhao, and Z. M. Zhang, "Resonance enhanced absorption in a graphene monolayer using deep metal gratings," J. Opt. Soc. Am. B **32**(6), 1176–1185 (2015).
24. K. Araki and R. Z. Zhang, "Plasmon-resonance emission tailoring of "origami" graphene-covered photonic gratings," Opt. Express **28**(15), 22791–22802 (2020).
25. K. Araki and R. Z. Zhang, "Mechano-Optical Resonant Emission by Edge Angle Modulation of Wrinkled Graphene on Plasmonic Metal Gratings," ACS Appl. Nano Mater. **4**(8), 8399–8407 (2021).
26. J. Xue, J. Sanchez-Yamagishi, D. Bulmash, P. Jacquod, A. Deshpande, K. Watanabe, T. Taniguchi, P. Jarillo-Herrero, and B. J. LeRoy, "Scanning tunnelling microscopy and spectroscopy of ultra-flat graphene on hexagonal boron nitride," Nat. Mater. **10**(1), 4 (2011).
27. X. Luo, T. Qiu, W. Lu, and Z. Ni, "Plasmons in graphene: recent progress and applications," Mater. Sci. Eng., R **74**(11), 351–376 (2013).
28. F. H. Koppens, D. E. Chang, and F.J. García de Abajo, "Graphene plasmonics: a platform for strong light–matter interactions," Nano Lett. **11**(8), 3370–3377 (2011).
29. Y. Francescato, V. Giannini, and S. A. Maier, "Strongly confined gap plasmon modes in graphene sandwiches and graphene-on-silicon," New J. Phys. **15**(6), 063020 (2013).
30. Z. H. Ni, H. M. Wang, J. Kasim, H. M. Fan, T. Yu, Y. H. Wu, Y. P. Feng, and Z. X. Shen, "Graphene thickness determination using reflection and contrast spectroscopy," Nano Lett. **7**(9), 2758–2763 (2007).

Optics EXPRESS

31. D. K. Efetov and P. Kim, "Controlling electron-phonon interactions in graphene at ultrahigh carrier densities," Phys. Rev. Lett. **105**(25), 256805 (2010).
32. R. S. Shishir, F. Chen, J. Xia, N. J. Tao, and D. K. Ferry, "Room temperature carrier transport in graphene," J. Comput. Electron. **8**(2), 43–50 (2009).
33. J. Fang, W. G. Vandenberghe, and M. V. Fischetti, "Microscopic dielectric permittivities of graphene nanoribbons and graphene," Phys. Rev. B **94**(4), 045318 (2016).
34. A. Laturia, M.L. Van de Put, and W.G. Vandenberghe, "Dielectric properties of hexagonal boron nitride and transition metal dichalcogenides: from monolayer to bulk," npj 2D Mater. Appl. **2**(1), 6–7 (2018).
35. K. Li, J. M. Fitzgerald, X. Xiao, J. D. Caldwell, C. Zhang, S. A. Maier, X. Li, and V. Giannini, "Graphene plasmon cavities made with silicon carbide," ACS Omega **2**(7), 3640–3646 (2017).